AIAA JOURNAL
Vol. 46, No. 9, September 2008

# How to Solve Compressible Multifluid Equations: A Simple, Robust, and Accurate Method

Meng-Sing Liou*
*NASA John H. Glenn Research Center at Lewis Field, Cleveland, Ohio 44135*
and
Chih-Hao Chang,† Loc Nguyen,‡ and Theo G. Theofanous§
*University of California, Santa Barbara, Santa Barbara, California 93106*

DOI: 10.2514/1.34793

**Solving multifluid equations of compressible multiphase flows has proven extremely demanding because of some peculiar mathematical properties such as nonhyperbolicity, nonconservative form, and stiffness due to disparity in fluid properties and flow scales. This paper gives several new contributions toward addressing difficulties arising from these properties. We first consider the mathematical issues concerning nonhyperbolicity and nonconservative form and establish their effects on the stability and convergence of numerical solutions. Then we present a new numerical method that is simple to implement without the need of employing the eigenstructure of the equations, which would be difficult to find for a general class of fluids. We show that our method properly removes numerical difficulties associated with the multifluid equations and it is capable of robustly and accurately calculating phenomena involving material and shock discontinuities and interactions between them for a range of typical multiphase problems of one and two space dimensions. Finally, the paper is completed with new information for ensuring hyperbolicity by an interfacial-pressure representation.**

## I. Introduction

MULTIPHASE flows, seen in a broad range of disciplines and applications, encompass many complex phenomena. Typically, the flow is under widely disparate conditions of pressure, flow speed, and material properties. Examples include breakup of droplets and their subsequent dispersal and phase changes involving cavitation, boiling, condensation, or freezing. Flows of such kinds are extremely complicated and they are usually described by two sets of balance equations, the so-called effective field models [1,2], resulting from averaging of the Navier–Stokes equations. Each set describes the motion of corresponding phase, with attendant transfer terms that account for the interactions between phases.

Numerically solving such systems becomes rather challenging because of the following factors:

1) The modeling of averaged terms cannot be expressed in conservation form.

2) The resulting system may become nonhyperbolic.

3) The physical problems of interest yield a stiff mathematical system when the material properties are of great disparity, such as water and air in which the acoustic impedance can differ by 4000 times.

As a result of factors 1 and 3, it is much more difficult to capture a shock wave or contact discontinuity in water than in the air, because a small variation in water density may induce large oscillations in the pressure field.

Presented as Paper 4456 at the 18th AIAA Computational Fluid Dynamics Conference, Miami, FL, 25–28 June 2007; received 25 September 2007; revision received 29 April 2008; accepted for publication 4 June 2008. 

*Senior Technologist, Computational Fluid Dynamics and Aeropropulsion; Meng-Sing.Liou@grc.nasa.gov.

†Assistant Researcher, Center for Risk Studies and Safety; chchang@engr.ucsb.edu.

‡Assistant Specialist, Center for Risk Studies and Safety; loc@engr.ucsb.edu.

§Professor and Director, Center for Risk Studies and Safety; theo@engr.ucsb.edu.

Previously, we proposed to use the stratified-flow concept to formulate numerical fluxes [3,4]; the stratified-flow model considers that different fluids are separated from each other *within* each computation cell (or control volume). As a result, this approach helps to clearly account for different types of numerical fluxes, either between like fluids or unlike fluids. The numerical flux between the same fluids (gas–gas or liquid–liquid) is calculated by the advection upstream splitting method AUSM$^+$-up scheme, and the numerical flux between different fluids (gas–liquid) is calculated by the exact Riemann solver. We have shown that this approach is effective in capturing complex phenomena with fluid interfaces and shock waves: notably, in the shock–bubble and shock–droplet interaction problems [4,5].

However, the use of an exact Riemann solver puts considerable limitations on the approach, for the following reasons:

1) Explicit analytical formulas in the form of Riemann invariants are not possible for a more realistic equation of state (EOS).

2) The Riemann solver can become considerably expensive when lots of iterations are invoked, which is usually the case.

On the other hand, approximate Riemann solvers, such as Roe's flux, require an explicit form of the eigenstructure of the hyperbolic system, which is also not available analytically for a general fluid, because the eigenvalues are the roots of a complicated quartic equation.

Hence, the present study especially aims at constructing a general flux formula that has at least the following properties:

1) It does not use the exact Riemann solver or rely on the eigenstructure of the equations.

2) It is easily applicable for complex EOS.

3) It is robust and accurate for resolving both shock wave and material (contact) discontinuities.

The construction of modern numerical methods for compressible flows has been entirely based on the premise that the mathematical system is hyperbolic. This condition has been known to be a necessary one for a *linear* system to render numerical calculations well-posed. However, it has not been demonstrated how ill-posedness due to nonhyperbolicity manifests itself in a *nonlinear* system and to what extent the numerical solution is devastated by it.

One of the peculiar properties associated with a two-fluid system is that the basic system is nonhyperbolic. To render the first-order system hyperbolic, it is natural to seek an augmentation with additional closure terms that are physics-based and expressed as first

derivatives in time or space. By adopting a closure model, known as interfacial pressure, we carry out an in-depth investigation with regard to hyperbolicity and study its numerical implications.

Finally, studies concerning the numerical implications of nonconservative terms have been conducted in mathematical analysis [6,7], but no direct evidence has been shown about its connection to stability or convergence. We shall also address this issue based on numerical evidence. Especially, we show that if this nonconservative term is not properly handled, serious repercussions in numerical solution can arise. Consequently, we propose a robust way for curing the difficulty.

## II. Effective Field Modeling: Two-Fluid Equations

In flow situations in which multiple material phases are found at scales that cannot be resolved by direct numerical simulation, one then resorts to describing the dynamics with the averaged coarse-grain models [1,2], collectively called effective field modeling (EFM), because they typically result from averaging (time, volume, or ensemble) of fundamental balance equations by considering different fluids. As in turbulence modeling, major difficulties also arise in finding appropriate closure forms for the interaction terms introduced by the averaging procedure. To fix our focus, we shall consider only the 1-D form of inviscid two-fluid EFM, expressed as follows:

$$\frac{\partial \mathbf{U}_k}{\partial t} + \frac{\partial \mathbf{F}_k}{\partial x} = \mathbf{P}_k^{\text{int}} + \mathbf{F}_k^{\text{vm}} + \mathbf{S}_k, \qquad k = 1, 2 \tag{1}$$

where

$$\mathbf{U}_k = \begin{bmatrix} \alpha_k \rho_k \\ \alpha_k \rho_k u_k \\ \alpha_k \rho_k E_k \end{bmatrix}$$

$$\mathbf{F}_k = \begin{bmatrix} \alpha_k \rho_k u_k \\ \alpha_k \rho_k u_k^2 \\ \alpha_k \rho_k u_k H_k \end{bmatrix} + \begin{bmatrix} 0 \\ \alpha_k p_k \\ 0 \end{bmatrix} \tag{2}$$

$$\mathbf{P}_k^{\text{int}} = \begin{bmatrix} 0 \\ p_k^{\text{int}} \frac{\partial \alpha_k}{\partial x} \\ -p_k^{\text{int}} \frac{\partial \alpha_k}{\partial t} \end{bmatrix}$$

As shown, these terms are similar to those of single-fluid equations, except with the volume fraction $\alpha_k$ included: $\mathbf{U}_k$ is a vector of conservative variables, $\mathbf{F}_k$ are the inviscid fluxes, and $\mathbf{S}_k$ are the source terms added to the system (for example, due to body forces, heat addition, mass addition via phase transition, etc.). There are two new terms in the effective field modeling: the so-called interfacial pressure $\mathbf{P}_k^{\text{int}}$ and virtual mass $\mathbf{F}_k^{\text{vm}}$, respectively, both characterizing macroscopic interactions between participating phases.

In the preceding 1-D EFM system (1), there are 12 unknowns [$\alpha_k$, $\rho_k$, $u_k$, $p_k$, $E_k$, and $p_k^{\text{int}}$ ($k = 1, 2$)] and a total of 9 equations with 6 partial differential equations (PDEs), 2 EOS, and 1 compatibility relation for volume fraction $\alpha_k$:

$$\sum_{k=1}^{2} \alpha_k = 1 \tag{3}$$

Hence, three more equations must be supplied. An often-used assumption is that the bulk pressures of all phases are equal (in equilibrium) [1,8]:

$$p_1 = p_2 \equiv p \tag{4}$$

Another condition is required for the consistency of interfacial pressures: namely, they must cancel out each other (equal in magnitude if no other stresses such as surface tension, viscous stresses, etc., are considered at the interface). Hence,

$$p_1^{\text{int}} = p_2^{\text{int}} \equiv p^{\text{int}} \tag{5}$$

The third condition is customarily provided by relating the interfacial pressure $p^{\text{int}}$ with the bulk pressure $p$ via a delta term (a finite jump). That is, the interfacial pressure is thought of as a departure from the local bulk pressure:

$$p^{\text{int}} = p - \delta p^* \tag{6}$$

where $\delta p^*$ will be specified subsequently.

For the hyperbolicity analysis, we shall ignore the source term because it typically does not involve derivatives of unknown variables. Based on our past investigations, we have concluded that various modelings for virtual mass proposed in the literature are either ineffective (requiring a nonphysically large value of coefficient) in yielding real-valued characteristics or give rise to adverse effects that are detrimental to stability and convergence of calculations. Because for the problems considered here (disperse flow with gas as the continuum phase), added (virtual) mass effects are negligible in any case and will not be dealt with here. Instead, we shall concentrate on the interfacial-pressure form, as originally advocated by Stuhmiller [9] and further expounded by us recently [10,11].

### A. Interfacial Pressure

Following Stuhmiller [9], the interfacial pressure $p^{\text{int}}$, expressed in terms of $\delta p^*$ in Eq. (6), is given in the following, for a liquid (denoted by subscript $l$) and gas (subscript $g$) system:

$$\delta p^* = \sigma \frac{\alpha_g \alpha_l \rho_g \rho_l}{\alpha_g \rho_l + \alpha_l \rho_g} w^2, \qquad w = u_l - u_g \tag{7}$$

Or, if we consider liquid and gas as dispersed and continuous phases, respectively, the preceding equation can be written in another form:

$$\delta p^* = C_p^* \alpha_l \rho_g w^2 \tag{8}$$

In the case of low relative fluid speed compared with the gas-phase speed of sound, $w^2 \ll a_g^2$, the necessary condition for hyperbolicity is found to be [9]

$$\sigma \geq 1 \quad \text{or} \quad C_p^* \geq 1 \tag{9}$$

However, when the relative velocity $w^2$ is not small compared with $a_g^2$, we showed [10] that the coefficients $\sigma$ and $C_p^*$ must be set sufficiently large to maintain hyperbolicity. Thus, we proposed a simple formula that is sufficient to guarantee hyperbolicity for all volume fractions, fluid densities, and speed conditions:

$$\delta p^* = \rho_g w^2 \tag{10}$$

This condition, although proper at high relative speed, is overly conservative when $\alpha_l \ll 1$ and $w^2 \ll a_g^2$, as evident from Eq. (8). A more precise condition has been recently developed [11]. An approximate analytical form of $C_p^*$, a function of variables $\alpha_k$, $w$, and $a_g$, is derived for particulate flows, under the condition that the parameter $\varepsilon = (1 + \alpha_g \rho_l / \alpha_l \rho_g)^{-1} \ll 1$. A summary of its details is given in Appendix A. Here, we list the approximate form:

$$C_p^* = \begin{cases} (1 - \alpha_g M_r^2)^{-1} & \text{if } M_r \leq 1.0 \\ \frac{1}{\alpha_l}\left(\frac{(1-M_r^2)^3}{27\varepsilon} + 1\right) & \text{if } 1 < M_r < \frac{1}{\sqrt{\alpha_g}} \\ 0 & \text{if } M_r \geq \frac{1}{\sqrt{\alpha_g}} \end{cases} \tag{11}$$

where $M_r = (u_c - u_d)/a_m$ is the relative Mach number based on a mixture speed of sound $a_m$ (see Appendix A). The interested reader should refer to the preceding cited reference for a thorough account of hyperbolicity and its implications in a wide range of benchmark problems.

### B. Equations of State

System (1) is closed with the provision of equations of state (EOS) of the fluids considered. We used the so-called stiffened-gas model [12] to approximately describe the liquid phase $l$, which is expressed as

$$p_l = \frac{\gamma_l - 1}{\gamma_l}\rho_l C_{p_l} T_l - p_\infty, \qquad e_l = \frac{C_{p_l}}{\gamma_l} T_l + \frac{p_\infty}{\rho_l} \tag{12}$$

where

$$\gamma_l = 2.8, \qquad C_{p_l} = 4186 \text{ J/(kg} \cdot \text{K)}, \qquad p_\infty = 8.5 \times 10^8 \text{ Pa} \tag{13}$$

This model is convenient for analysis because it differs only slightly from the ideal-gas EOS. As a result, it gives rise to considerable simplification in formulation and coding because the gas phase (modeled as an ideal gas) is only a special case of the stiffened-gas model, by simply setting $p_\infty = 0.0$ and $\gamma_g = 1.4$. Although it is cautioned that the stiffened-gas model lacks accuracy for representing the behavior of liquid, it is quite sufficient for our purposes here.

Aside from presenting a new numerical method, another important aspect of this paper is to bring out numerical issues pertaining to the multifluid equations under consideration, which is discussed next.

## III. Numerical Issues

A close observation of the EFM equations reveals three distinguished features that require further elaboration:

1) The interfacial-pressure and the virtual-mass (not considered here) terms can only be cast in nonconservative form.

2) The system may become nonhyperbolic.

3) The system becomes stiff with vastly different fluid properties.

These factors can have serious repercussions on numerical solutions and they are the primary concerns that motivated the present study.

### A. Nonconservative Terms

It is known that the standard methods that correctly solve systems in conservation form can fail badly when used in a nonconservative system, even in a simple situation. An example is shown in Fig. 1, in which the nonconservative term is approximated by a seemingly reasonable centered scheme; however, it results in a catastrophic departure from the equilibrium state across a stationary contact discontinuity. This may be understood from the following simple analysis; the momentum equation in this case reduces to

$$\frac{\partial p\alpha_k}{\partial x} = p\frac{\partial \alpha_k}{\partial x} \tag{14}$$

That is, the balance between the conservative and nonconservative pressure terms must be maintained at the discrete level as well (or at the so-called pressure no-disturbance condition [13]). The mathematical questions concerning existence, uniqueness, and stability of solution of nonconservative hyperbolic systems have attracted extensive studies, yet the theory remains less conclusive than for conservative systems [6,7].

### B. Hyperbolicity

With $\mathbf{P}^{\text{int}}$ or $\mathbf{F}^{\text{vm}}$ expressed in terms of first derivatives, Eq. (1) can be rewritten, in general, as

$$\frac{\partial \mathbf{U}_k}{\partial t} + \frac{\partial \mathbf{F}_k}{\partial x} = \mathbf{C}_{t,k}\frac{\partial \mathbf{U}_k}{\partial t} + \mathbf{C}_{x,k}\frac{\partial \mathbf{U}_k}{\partial x} \tag{15}$$

With $\mathbf{C}_{t,k} = \mathbf{C}_{x,k} = 0$, the system reduces to two decoupled independent fluid systems and they are individually hyperbolic, the same as a single-fluid system, but they are useless for describing the dynamics of two fluids. However, if they are nonvanished, there is no guarantee that the resulting system will have real-valued characteristics; in fact, this coupling term holds the key to fundamentally changing the hyperbolicity of the system. Numerous studies have been devoted to addressing topics concerning nonhyperbolicity: some studying the hyperbolicity nature of specific EFM equations for multiphase flows and some analyzing whether a solution exists uniquely and stably in nonhyperbolic equations [14,15]. Similar to the case of nonconservative form, the mathematical theory for nonhyperbolic nonlinear systems remains incomplete.

It is known that there is a strong connection between nonhyperbolicity and ill-posedness of a PDE system. In Fig. 2, we see there is a strong spike at the contact discontinuity for the long-standing faucet problem; the spike gets larger as the grid size decreases, eventually leading to a complete failure. Hence, in many previous studies [9,16,17], the focus has been directed toward how to render the system hyperbolic, primarily by including terms under the categories of interfacial pressure and virtual (added) mass. The justification was that some physics have been lost during the averaging, and thus inclusion of more details of the subscale flow could result in real-number characteristics.

Meanwhile, to overcome difficulties arising from stability and numerical oscillations, it is common to use lower-order schemes or other smoothing approaches (such as adding pressure relaxation terms [18]). Both amount to adding numerical dissipation, thus severely decreasing accuracy of results with smearing.

To get a better understanding of the nonhyperbolicity issue on accuracy, stability, and convergence of the solution, we numerically investigated its effects and shall discuss the results later in Sec. IV. However, we must first establish a reliable numerical method for solving the system to assess the numerical effects.

It is noted that even after the system has been rendered hyperbolic for well-posedness, the eigensystem of the multifluid model is still very complicated and, in general, does not have a closed form. The conventional Roe or Godunov types of schemes, which essentially

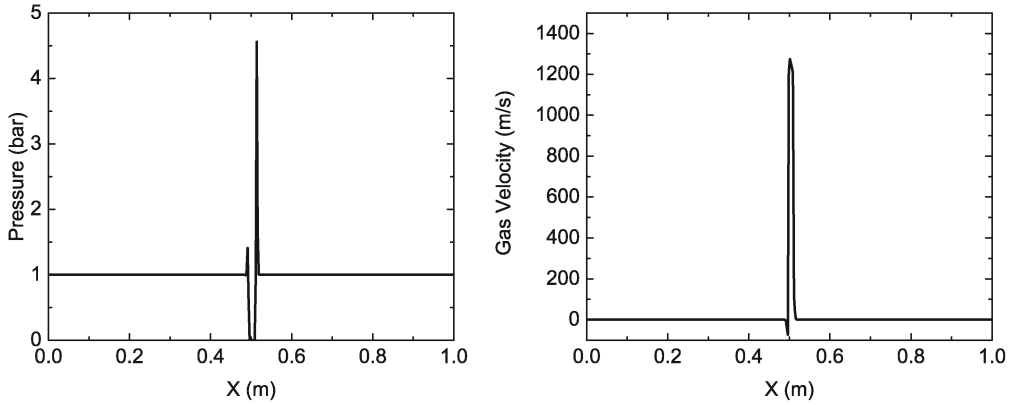


**Fig. 1 Contact discontinuity: pressure (left) and velocity (right); $p\partial\alpha/\partial x$ is calculated by central differencing; severe oscillations lead to eventual failure of solution.**

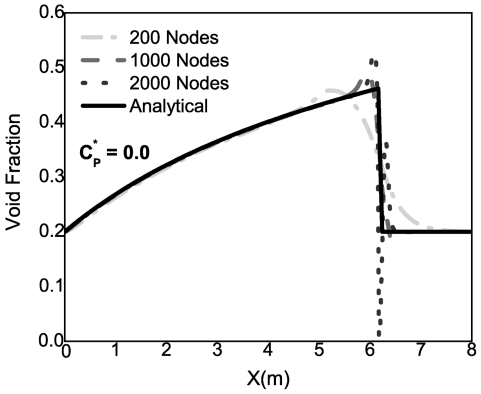


**Fig. 2 Solutions of a nonhyperbolic system as demonstrated in the Faucet problem; solutions are divergent as errors increase with decreasing grid spacing.**

rely on the availability of explicit forms of eigenvalues and eigenvectors, are ruled out. Instead, we are seeking an alternative approach, which we will give its detail in Sec. IV.

### C. Stiffness Because of Disparate Scales

For the types of multiphase flows of interest to us, large disparities in scales are almost always present between phases, typically resulting from density ratios of $\mathcal{O}(10^3)$ and speed ratios of $\mathcal{O}(10^2 \sim 10^3)$. Although the stiffness of the mathematical system is not traceable to a specific term in Eq. (1), it exists largely due to physical problems considered. That is, it is of a physics nature, but gives rise to numerical difficulties that must be dealt with by numerical methods. An example is shown in Fig. 3 for a water shock-tube problem in which the pressure ratio is 10:1 but the water velocity generated is only $\mathcal{O}(0.1)$ m/s [or a Mach number of $\mathcal{O}(10^{-4})$]. The result by AUSM$^+$ without proper scaling for low Mach numbers is totally erratic, producing odd–even oscillations in the middle constant-pressure region, as evident in the velocity profile, and serious irregularities near the shock and rarefaction waves.

## IV. Numerical Method

For solving a two-fluid flow system, in this section we present a new multiphase AUSM method that has several key features:

1) It does not require knowing the details of waves structure (eigenstructure), but still maintains the idea of properly treating both the linear and nonlinear waves, manifested as convective and pressure fields, respectively.

2) It properly treats nonconservative terms.

3) It is capable of robustly and accurately dealing with flows of disparate scales, such as a large acoustic impedance ratio or a low Mach number region embedded in a high-speed flow.

In what follows, we first use the control-volume formulation to derive discrete balance equations. This way is found to be extremely instructive for the following reasons:

1) It makes a clear physical connection to the very idea of the AUSM concept for constructing numerical fluxes at boundaries of the control volume, in which the convection and pressure are viewed as separate processes.

2) It also sheds a clear light on the interpretation of the nonconservative terms, thus suggesting its treatment.

Previously, we used the stratified-flow concept [8] to develop a robust and accurate numerical method for discretizing the conservation laws [5]. The stratified-flow model divides a bulk fluid into separate fluids according to a characterizing property (typically the volume fraction). It fits in nicely with the finite volume framework and it gives a clear clue as to how the conservation laws can be applied to each region of a fluid domain. In fact, using this concept, we can directly construct a discrete set of balance equations and recover their continuous counterparts after taking the limit of small mesh size (in Taylor's series expansion).

To apply the stratified-flow model to multifluid flow, we first divide the control volume into different fluid regions according to the volume-fraction distribution and then identify interfaces between the same and different fluids at the control surfaces, as illustrated in Fig. 4.

In Fig. 4, the volume-fraction function $\alpha_k$ is used to define individual control volumes of gas $\overline{acgh}$ and liquid $\overline{cdeg}$ within the mesh cell $j$. It is assumed that $\alpha_k$ is piecewise continuous within each cell and allowed a jump at the cell boundaries $j \pm 1/2$. Balance of mass, momentum, and energy can be accounted for at the cell boundaries, as in the single-fluid flow, except that the interactions in the form of mass, momentum and energy transfer at the interface between two fluids *within* the cell must be added. For our study, we exclude phase transition at the fluid interface and viscous effects, and thus only pressure force takes effect in the momentum and energy equations. The pressure that acts at the phase interface $\overline{cg}$ need not be the same as the bulk-fluid pressure and is denoted as interfacial pressure $p^{\text{int}}$. This pressure force, directed along the normal to the segment $\overline{cg}$, gives rise to a component in the $x$ direction, $p^{\text{int}}\Delta\alpha_k$, where $\Delta\alpha_k$ is the change of $\alpha_k$ within the cell.¶ For the energy balance, the work produced by the interfacial pressure is simply associated with the volume (fraction) change between consecutive times.

Using $\delta_t(\cdot)^n = (\cdot)^{n+1} - (\cdot)^n$ as the time-difference operator, we now express the discrete balance equations for fluids in control volume $j$ as follows:

$$\frac{1}{\Delta t}\delta_t \begin{bmatrix} \upsilon_k\rho_k \\ \upsilon_k\rho_k u_k \\ \upsilon_k\rho_k E_k \end{bmatrix}_j + \begin{bmatrix} \dot{m}_k\alpha_k \\ \dot{m}_k\alpha_k u_k \\ \dot{m}_k\alpha_k H_k \end{bmatrix}_{j-1/2}^{j+1/2} + \begin{bmatrix} 0 \\ \alpha p \\ 0 \end{bmatrix}_{j-1/2}^{j+1/2} - \bar{p}_j \begin{bmatrix} 0 \\ \Delta_j\alpha_k \\ \frac{1}{\Delta t}\delta_t\upsilon_k \end{bmatrix} = 0 \tag{16}$$

where

$$\upsilon_{kj} = \alpha_k \Delta x_j \tag{17}$$

is the volume occupied by the $k$ fluid in cell $j$, and

$$\dot{m}_k = \rho_k u_k \tag{18}$$

is the mass flux. The second and third terms express balance of convective fluxes and pressure force *at* the cell boundaries $j + 1/2$ and $j - 1/2$; they are exactly in conservative form. The last term stems from the exchange of momentum and energy between fluids (phases) *within* the cell by the pressure force $\bar{p}_j$ that is averaged over the interface $\overline{cg}$ and is in nonconservative form.

It is from this construction that the meaning and origin of the nonconservative term in Eq. (2) now becomes clear: it is due to the internal interactions between phases via pressure forces. Thus, we may assign $\bar{p} = p^{\text{int}}$. It is noted that these terms from both fluids cancel out each other exactly, thus resulting in a complete conservative form of equations for the *mixture*, albeit still in nonconservative form for individual phases.

*Remark*. It can be easily shown that the preceding discrete system reduces to the continuous counterpart as the mesh size and time step vanish. Hence, both systems are equivalent. However, the discrete system is useful because it sheds light on how to construct a numerical method for the two-fluid system.

The key components to solving the discrete equations essentially boil down to the definitions of 1) mass flux $\dot{m}_{j\pm1/2}$ at the cell boundaries, 2) pressure flux $p_{j\pm1/2}$, and 3) the nonconservative term (specifically, $\Delta_j\alpha_k$). The first two naturally fall in the framework of

¶It is interesting to note that the volume-fraction function (as manifested by $\overline{gh}$) may be thought of as an area function in 1 D nozzle flow in which the area change also appears in nonconservative form, but as a given function.

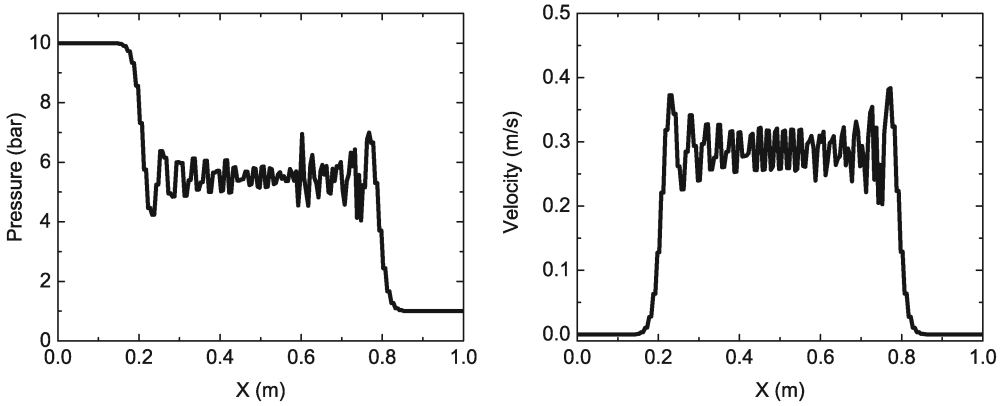


**Fig. 3 Solutions of the underwater shock-tube problem without accounting for low Mach number correction; the odd–even oscillations bounce between two branches in the velocity profile.**

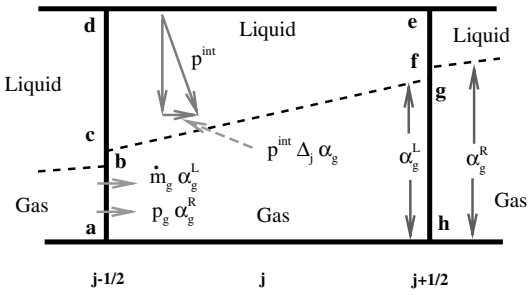


**Fig. 4 Illustration of the one-dimensional stratified flow.**

the AUSM family [19–21]. In fact, it has been shown to be the cornerstone of several extensions for multifluid equations [5,22,23]. However, the treatment of the nonconservative term is new. Here, the area-function analogy is no longer applicable because it is a given function, not part of unknowns. Thus, care must be taken to ensure consistency; otherwise, erratic result (as shown in Fig. 1) can arise. In what follows, these details will be given.

### A. Convective Fluxes

The basic idea for constructing a numerical flux for convective terms follows that in AUSM$^+$ [20]. However, because the velocities and densities of both fluids can be of exceedingly different [say, by a factor of $\mathcal{O}(10^3)$], proper scaling for coupling velocity and pressure fields must be exercised. To this end, the scaling given in AUSM$^+$-up [5,21] is proper for the physical problems of interest.

For illustration, we express the convective flux at interface $j+1/2$, denoted by subscript $1/2$, by

$$\mathbf{f}^{(c)}_{k,1/2} = \dot{m}_{k,1/2}\boldsymbol{\psi}_{k,L/R}, \qquad \boldsymbol{\psi}_k = (\alpha_k, \alpha_k u_k, \alpha_k H_k)^T \tag{19}$$

where $\dot{m}_{k,1/2}$ is the common mass flux.

Simple upwinding is applied to the quantities with subscripts $L$ and $R$, respectively, referring to the left and right states with respect to the cell boundary $1/2$:

$$\boldsymbol{\psi}_{k,L/R} = \begin{cases} \boldsymbol{\psi}_{k,L} & \text{if } \dot{m}_{k,1/2} > 0 \\ \boldsymbol{\psi}_{k,R} & \text{otherwise} \end{cases} \tag{20}$$

The mass flux is defined as

$$\dot{m}_{k,1/2} = u_{k,1/2}\rho_{k,L/R} = u_{k,1/2}\begin{cases} \rho_{k,L} & \text{if } u_{k,1/2} > 0 \\ \rho_{k,R} & \text{otherwise} \end{cases} \tag{21}$$

The most intricate part lies in $u_{k,1/2}$, for which the definition is as follows:

$$u_{k,1/2} = a_{1/2}[\mathcal{M}^+_{(4)}(M_{k,L}) + \mathcal{M}^-_{(4)}(M_{k,R}) + M_{pk}] \tag{22}$$

where we define

$$M_{k,L/R} = \frac{u_{k,L/R}}{a_{1/2}} \tag{23}$$

$$M_{pk} = -K_p \max(1-\bar{M}^2_k, 0)\frac{p_R - p_L}{\rho_{k,1/2}a^2_{1/2}}, \qquad 0 \le K_p \le 1 \tag{24}$$

with

$$\rho_{k,1/2} = (\rho_{k,L} + \rho_{k,R})/2, \qquad \bar{M}^2_k = \left(M^2_{k,L} + M^2_{k,R}\right)/2 \tag{25}$$

The speed of sound $a_{1/2}$ can be defined in several ways. The most important thing to observe is that a common (numerical) speed of sound should be used to define $M_L$ and $M_R$ and for both fluids. The latter condition is different from that in Chang and Liou [5], in which different sound speeds are used for different fluids. The following definitions have been used with success:

$$a_{1/2} = \tfrac{1}{2}(a_{g,1/2} + a_{l,1/2}) \tag{26}$$

or

$$a_{1/2} = \sqrt{\left[\frac{a^2_g a^2_l(\rho_g + \rho_l)}{\rho_g a^2_l + \rho_l a^2_g}\right]_{1/2}} \tag{27}$$

The split Mach number functions $\mathcal{M}^{\pm}_{(4)}$ are

$$\mathcal{M}^{\pm}_{(4)}(M) = \begin{cases} \mathcal{M}^{\pm}_{(1)} & \text{if } |M| \ge 1 \\ \mathcal{M}^{\pm}_{(2)}(1 \mp 2\mathcal{M}^{\mp}_{(2)}) & \text{otherwise} \end{cases} \tag{28}$$

where

$$\mathcal{M}^{\pm}_{(1)}(M) = \tfrac{1}{2}(M \pm |M|), \qquad \mathcal{M}^{\pm}_{(2)}(M) = \pm\tfrac{1}{4}(M \pm 1)^2 \tag{29}$$

### B. Pressure Fluxes

The pressure flux is defined as

$$p_{k,1/2} = \mathcal{P}^+_{(5)}(M_{k,L})p_L + \mathcal{P}^-_{(5)}(M_{k,R})p_R + P_{uk} \tag{30}$$

where the velocity coupling term is

$$P_{uk} = -K_u\mathcal{P}^+_{(5)}(M_{k,L})\mathcal{P}^-_{(5)}(M_{k,R})\rho_{1/2}a_{1/2}(u_{k,R} - u_{k,L}), \qquad 0 \le K_u \le 1 \tag{31}$$

and the split pressure functions are

$$\mathcal{P}^{+}_{(5)}(M) = \begin{cases} \frac{1}{M}\mathcal{M}^{\pm}_{(1)} & \text{if } |M| \ge 1 \\ \mathcal{M}^{\pm}_{(2)}[(\pm 2 - M) \mp 3M\mathcal{M}^{\mp}_{(2)}] & \text{otherwise} \end{cases} \tag{32}$$

Although the pressure at the cell boundary $j+1/2$ is the same with respect to the same fluid, the total amount to the left cell ($j$) is

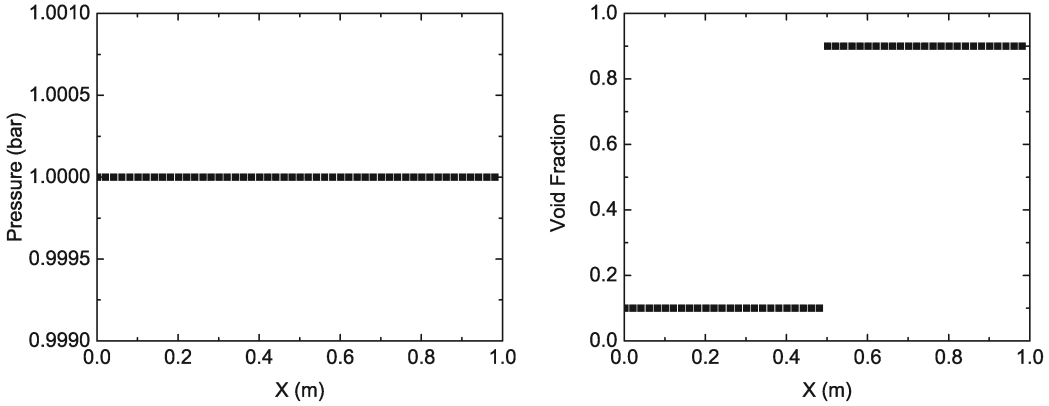


**Fig. 5 Contact discontinuity by a well-balanced discretization of pressure terms [Eqs. (33–35)], resulting in an exact solution.**

different from that to the right cell $(j+1)$ because $\alpha_{1/2,L} \neq \alpha_{1/2,R}$. They are given as follows.

For the $j$ cell,

$$(\alpha p)_{k,1/2}(j) = \alpha_{k,1/2,L} p_{k,1/2} \tag{33}$$

For the $j+1$ cell,

$$(\alpha p)_{k,1/2}(j+1) = \alpha_{k,1/2,R} p_{k,1/2} \tag{34}$$

Again, notice two values of $\alpha$ at $1/2$. The main point to note is that the force is applied at the control surfaces relevant to the specific cell under consideration of balance.

### C. Nonconservative Fluxes

The last term in Eq. (16) must be treated carefully so that the pressure nondisturbance condition (14) is satisfied for a stationary contact/interface discontinuity. Based on the stratified-flow concept, shown in Fig. 4, a clue is clearly suggested that the pressure is exerted at the phase interface *within the cell only*:

$$\Delta_j \alpha_k = \alpha_{k,j+1/2,L} - \alpha_{k,j-1/2,R} \tag{35}$$

*Lemma*. The pressure nondisturbance relation [Eq. (14)] is satisfied exactly by the flux formulas [Eqs. (33–35)] for a stationary contact/interface discontinuity ($u = 0$ and $p =$ constant) under all void and density conditions. Hence, by virtue of

$$\mathbf{f}^{(c)}_{j+1/2} = 0 \quad \forall\, j$$

the stationary contact discontinuity is preserved indefinitely.

The proof is straightforward and thus omitted here. Figure 5 shows that the calculation indeed confirms the preceding property. The pressure in an expanded scale stays constant throughout.

### D. Time Integration and Decoding of Conservative Variables

Here, the discretization of the first term in Eq. (16) is done explicitly, as usual. However, there are several choices for treating the time derivative of the fourth term in the energy equations. First, it can be frozen during the current time stepping and thus regarded as a source term:

$$p^{\text{int}} \delta_t \alpha_k^n = p^{\text{int}}(t^n)(\alpha_k^n - \alpha_k^{n-1}) \tag{36}$$

From the energy equation, we get the total energy at the new time level:

$$\mathcal{U}_{3_k}^{n+1} = (\alpha\rho E)_k^{n+1} = (\alpha\rho E)_k^n - \frac{\Delta t}{\Delta x}\left[\dot{m}_k^n \alpha_k^n H_{k,L/R}^n\right]_{j-1/2}^{j+1/2} + p^{\text{int}}(t^n)(\alpha_k^n - \alpha_k^{n-1}) \tag{37}$$

By relating $\mathcal{U}_3$ to other conservative variables $\mathcal{U}_1 = \rho\alpha$ and $\mathcal{U}_2 = \rho\alpha u$ at the same time level, we get updated volume fractions (hereafter, we drop the superscript $n+1$, for simplicity):

$$\begin{gathered} \alpha_k = \frac{\mathcal{A}_k}{p + a_k} \\ \mathcal{A}_k = (\gamma_k - 1)\left(\mathcal{U}_{3,k} - \frac{\mathcal{U}_{2,k}^2}{2\mathcal{U}_{1,k}}\right) \\ a_k = (\gamma p_\infty)_k \\ k = 1, 2 \end{gathered} \tag{38}$$

The compatibility relation $\alpha_1 + \alpha_2 = 1$ provides the equation for obtaining $p$ from a quadratic equation; the physically admissible root is

$$p = \tfrac{1}{2}(b + \sqrt{b^2 + 4c}) \tag{39}$$

where

$$b = \sum_{k=1}^{2}(\mathcal{A}_k - a_k), \qquad c = a_1\mathcal{A}_2 + a_2\mathcal{A}_1 - a_1 a_2 \tag{40}$$

Another approach is taken by including $p^{\text{int}}\partial\alpha_k/\partial t$ in the updating procedure. There are two slight variations in this category: the first one treats this term quasi linearly (i.e., fixing $p^{\text{int}}$ at current time $t^n$), and the second one treats it nonlinearly, in which $p^{\text{int}}$ is desired to be at $t^{n+1}$ by iteration. Both can be written in the same framework:

$$p^{\text{int}} \delta_t \alpha_k^n = p^{\text{int}}(t^*)(\alpha_k^{n+1} - \alpha_k^n), \qquad t^* = t^n \quad \text{or} \quad t^{n+1} \tag{41}$$

Again, the update of the energy equation gives, with $p^{\text{int}*} = p^{\text{int}}(t^*)$

$$\hat{\mathcal{U}}_{3,k} = \mathcal{U}_{3,k}^{n+1} + p^{\text{int}*}\alpha_k^{n+1} = \mathcal{U}_{3,k}^n + p^{\text{int}*}\alpha_k^n - \frac{\Delta t}{\Delta x}\left[\dot{m}_k^n \alpha_k^n H_{k,L/R}^n\right]_{j-1/2}^{j+1/2} \tag{42}$$

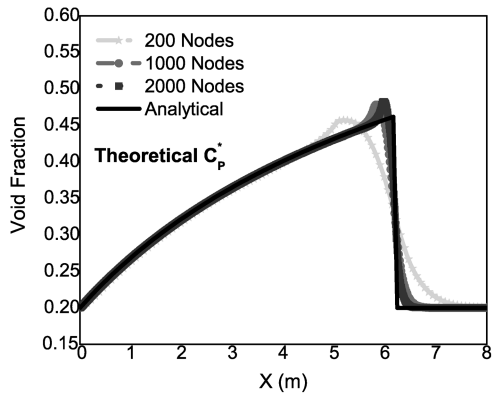


**Fig. 6 Solutions for the faucet problem obtained from the hyperbolized system; grid convergence is also evident.**

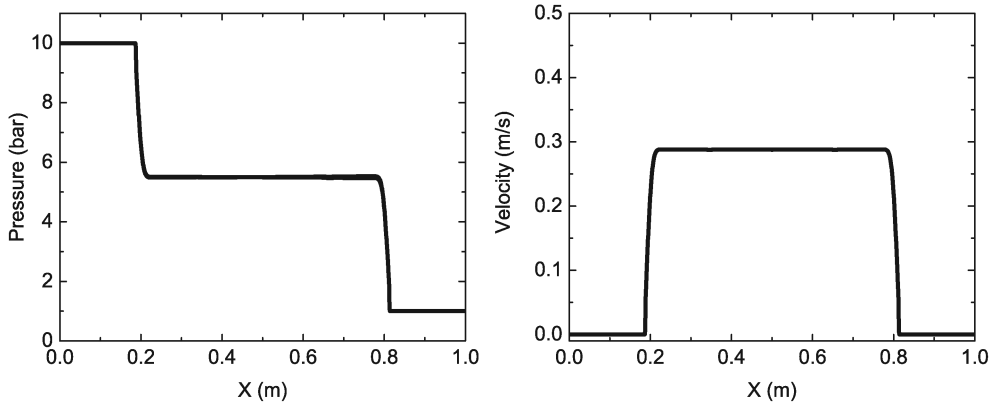


**Fig. 7 Underwater shock-tube problem, with proper scaling for low Mach number correction, in contrast to that given in Fig. 3; 200 nodes.**

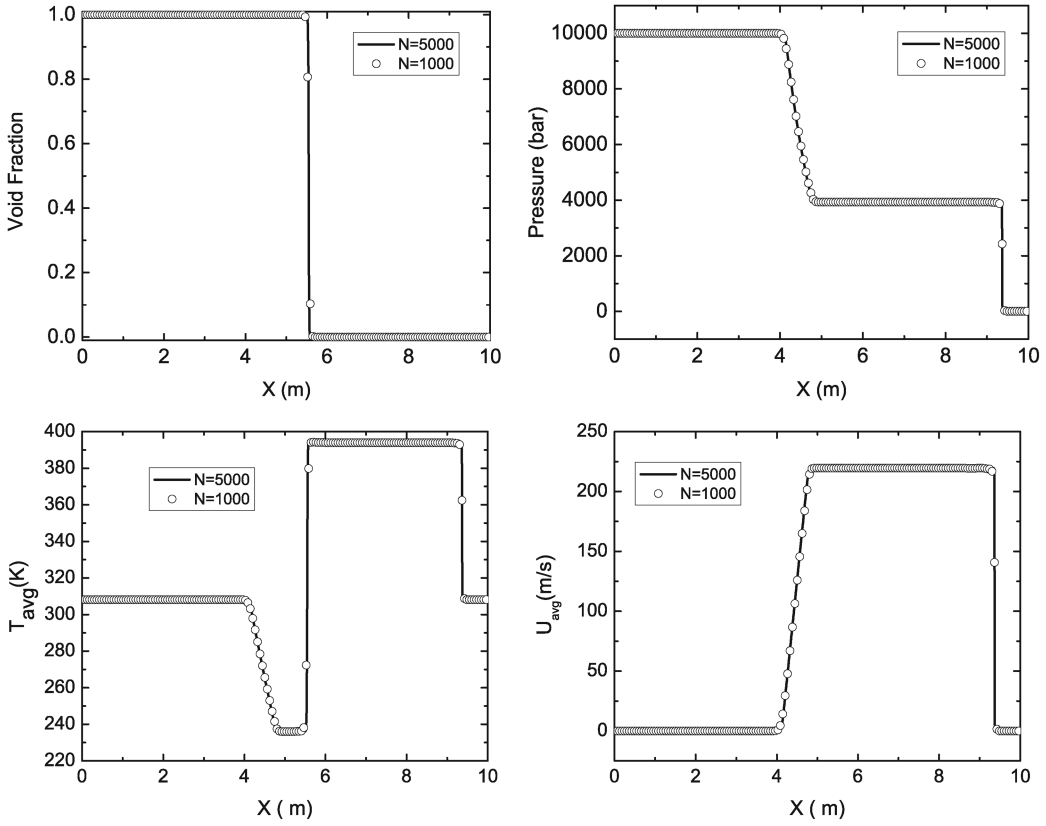


**Fig. 8 Air/water shock-tube problem, showing grid convergence in which the solution of $N = 1000$ is plotted every sixth point for clarity.**

$$\hat{\mathcal{U}}_{3,k} = \alpha_k^{n+1}\left[\frac{p^{n+1} + a_k}{\gamma_k - 1} + p^{\text{int}*}\right] + \frac{\mathcal{U}_{2,k}^2}{2\mathcal{U}_{1,k}} \tag{43}$$

and

$$\begin{aligned} \alpha_k^{n+1} &= \frac{\hat{\mathcal{A}}_k}{p^{n+1} + \hat{a}_k} \\ \hat{\mathcal{A}}_k &= \mathcal{A}_k + \alpha_k^{n+1}(\gamma_k - 1)p^{\text{int}*} \\ \hat{a}_k &= a_k + (\gamma_k - 1)p^{\text{int}*} \end{aligned} \tag{44}$$

The pressure at $t^{n+1}$ is then given exactly by the same formula as in Eq. (39), except the coefficients $b$ and $c$ are altered by substitution of $(\mathcal{A}, a)_k$ with $(\hat{\mathcal{A}}, \hat{a})_k$.

The second variation requires only an update of $p_k^{\text{int}*}$ in an inner loop during the time step $\Delta t = t^{n+1} - t^n$ until a specified tolerance is met. Each iteration involves a negligible amount of calculations and takes only a few iterations to reduce changes to the order of $10^{-15}$.

## V. Results and Discussion

A computer code based on the preceding described method has been developed; it is coined ARMS (all-regime multiphase flow simulator). It is Cartesian-grid based, has a solution adaptation capability using the SAMRAI (structured adaptive mesh refinement application infrastructure)** library, and is written for parallel computing. It is continuously being enhanced to include various physical modelings. The code has been extensively validated and used for various applications, and detailed documentation is available [24]. In this section, we shall demonstrate the capability of the preceding numerical method for a variety of problems to address the following numerical issues described in the previous section: 1) solution instability due to nonhyperbolicity, 2) effect of solution convergence by hyperbolicity, 3) effect of nonconservative terms, and 4) accuracy and robustness of the present method under extreme conditions.

**Data available online at http://www.llnl.gov/CASC/SAMRAI [retrieved 10 July 2008].

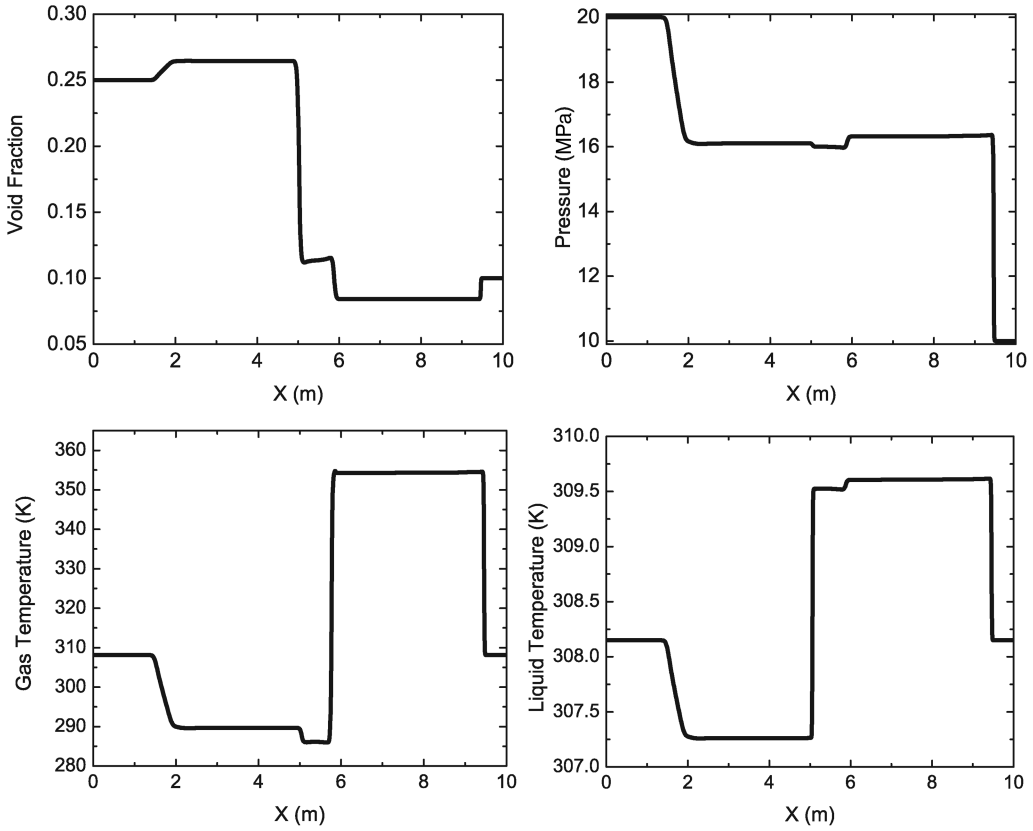


**Fig. 9 Two-fluid shock-tube problem [16]: an air/water mixture of different states initially separated at $x = 5$ evolves into a profile of five constant states separated by shock wave, contact, and rarefaction waves.**

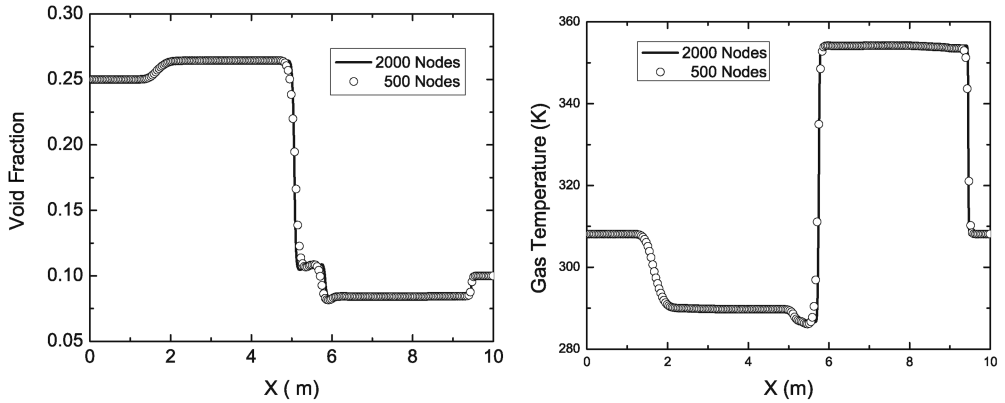


**Fig. 10 Grid convergence study of a hyperbolic system in which the solution of $N = 500$ is plotted every third point.**

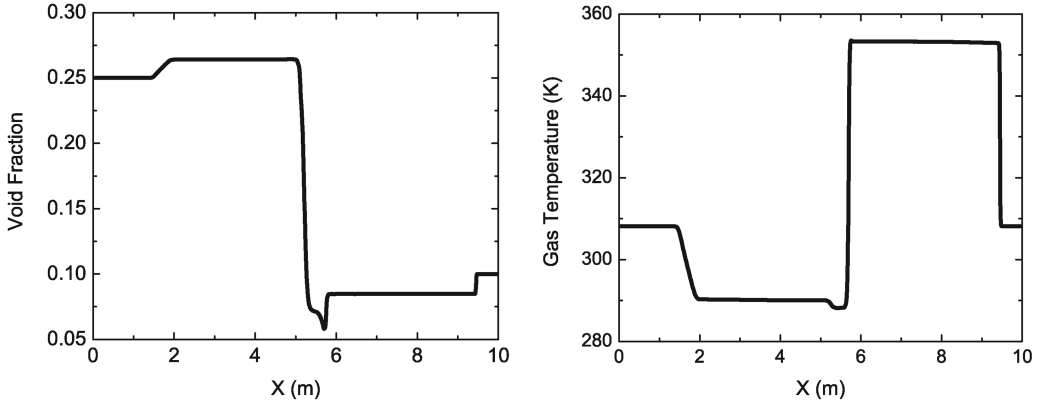


**Fig. 11 Effect of nonhyperbolicity on the solution.**

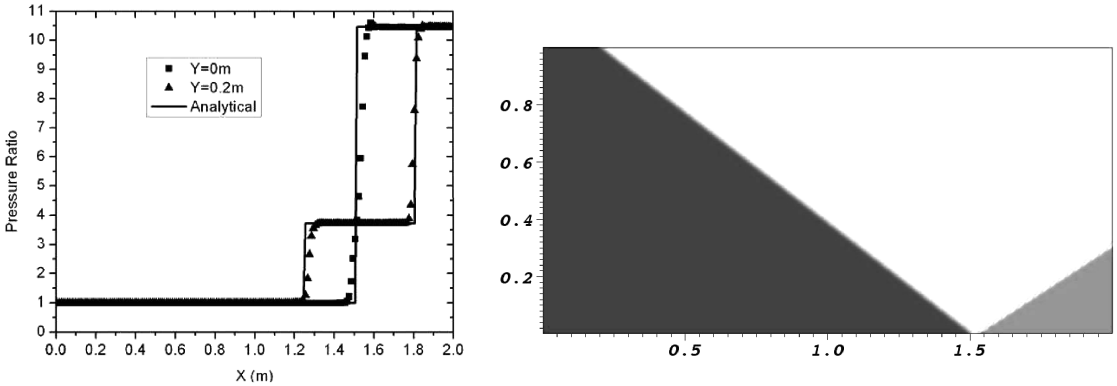


**Fig. 12 Two-fluid oblique shock wave problem.**

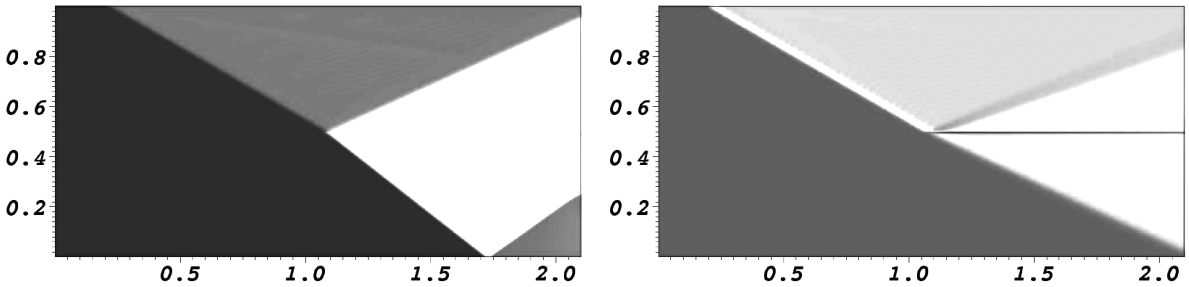

**Fig. 13 An oblique shock wave impinges on two-layer fluids.**

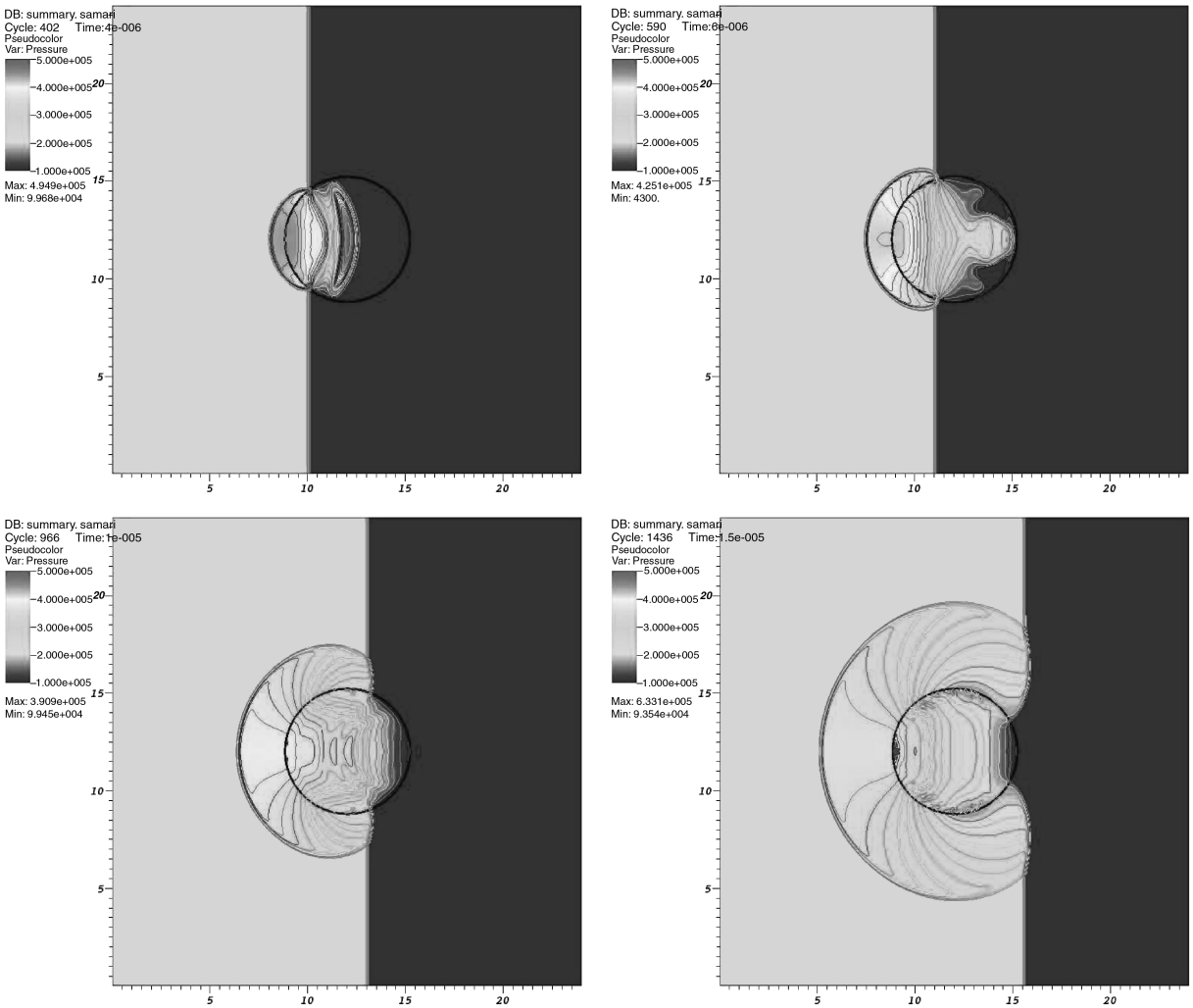


**Fig. 14 Evolution of pressure contours caused by a shock moving at $M_{sh} = 1.47$ toward a droplet at $t = 4$, 6, 10, and 15 $\mu$s.**

### A. Faucet Problem

After endowing the system with a sufficient amount of interfacial pressure, the system becomes hyperbolic and the numerical solution becomes well-behaved. In Fig. 6, the solution remains stable and converges as the grid size is refined, in stark contrast to that shown in Fig. 2.

### B. Shock-Tube Problems

We demonstrate the robustness of the present method for handling a stiff-liquid shock-tube problem. The disastrous results displayed in Fig. 3 are now completely eradicated. In contrast, the solution in Fig. 7 becomes absolutely well-behaved after being administered a proper scaling of low Mach number correction. It is interesting to note that when a liquid is considered, the rarefaction wave becomes very steep, as much as across the shock wave, owing to its high acoustic impedance.

In the next shock-tube problem, both air and water are separated initially and water is driven by air according to the following initial condition:

$$(p,\ \alpha_g,\ u_k,\ T_k)_L = (10^9\text{Pa},\ 1-\epsilon,\ 0\ \text{m/s},\ 308.15\ \text{K})$$
$$(p,\ \alpha_g,\ u_k,\ T_k)_R = (10^5\ \text{Pa},\ \epsilon,\ 0\ \text{m/s},\ 308.15\ \text{K})$$
$$k = 1, 2$$

where $\epsilon = 1.0 \times 10^{-7}$. The results on grids of 1000 and 5000 points are presented in Fig. 8; for clarity, the solution of 1000 nodes (denoted by circles) is plotted every sixth point, clearly demonstrating convergence of solutions.

A strong shock is transmitted into the liquid phase and a rarefaction wave is reflected back into the air phase. The flow features are resolved sharply, and the solution remains stable as the grid is refined. The reverse configuration in which the air is driven by the water was also computed and the results, not shown here due to the space limitation, behaved as well as those in Fig. 8.

Another very challenging problem is given by Toumi [16] in which a diaphragm initially separates two regions of fluids at different conditions: the left region has 25% of gas in volume and the right has 10%. This, after $t > 0$, develops into a flow with many intermediate waves associated with each fluid, demarcating uniform states between them. Figure 9 displays the profiles of different variables to show the rich structures of the solution; there are five distinctly constant states in all variables. Leading in both directions are the shock and rarefaction waves, respectively, and situated in the middle is a faint constant state bounded by two material waves, separately associated with liquid (at $x \approx 5$) and gas ($x \approx 6$) phases. The current method again performs well for this case. Next, we demonstrate the grid convergence in Fig. 10, in which the flow structures remain identical in magnitudes and locations between two solutions of different grid sizes, except the coarse grid exhibiting loss of sharpness.

Finally, the effect of nonhyperbolicity is displayed in Fig. 11; a noticeable difference from that of the hyperbolized solution occurs in the middle region of contact discontinuity.

### C. Oblique Shock Wave Problem

In this section, we show some representative 2-D cases. First, we calculated the solution for an oblique shock wave propagating in a homogeneous mixture of liquid and gas. Figure 12 shows the pressure contours and the pressure distributions, which are seen to be in good agreement with the analytical solution, with the shock wave captured at the correct location and strength.

Next, we consider that an oblique shock wave enters a two-layer stratified fluid, either the top layer with more gas volume (90 and 10% on the top and bottom, respectively) or the reverse. The left plot in Fig. 13 shows the pressure contours of the shock wave entering from the light layer (90% is air) to the heavy one, revealing the transmitted and reflected shock waves at the fluid interface. It is interesting to note the similarity between the shock wave and light in this regard. The right plot shows the result of the reverse situation, in which the top layer is heavy. Here, the shock wave is reflected as an expansion wave from the interface. Understanding this problem helps to interpret a more complex situation arising from shock wave and droplet interactions.

### D. Two-Dimensional Water Drop/Column Impinged by a Shock Wave

Here, we present results for a 2-D water column (diameter of 6.4 mm) subject to a shock wave moving at $M_{\text{sh}} = 1.47$. Again, the water phase is described by the stiffened-gas equation of state. The calculation was performed on a Cartesian grid with a grid spacing of 160 nodes per diameter. The volume fraction of the cells intersected by the interface is calculated according to the area occupied by either phase. The initial flow conditions are set up as follows for $k =$ air and water:

Before the shock,

$$p = 1.0\ \text{bar}, \qquad u_k = v_k = 0\ \text{m/s}, \qquad T_k = 293.15\ \text{K} \tag{45}$$

Behind the shock,

$$p = 2.35438\ \text{bar}, \qquad u_k = 225.86$$
$$v_k = 0\ \text{m/s}, \qquad T_k = 381.85\ \text{K} \tag{46}$$

The pressure contours at several representative time instants are given in Fig. 14. After impacting on the water column, the incident shock wave is transmitted into the water and simultaneously diffracts around the column as though it passed over a solid object. Because of higher sonic speed in water, the transmitted pressure wave proceeds faster inside the water region than the shock wave outside, clearly seen at $t = 4$ and 6 $\mu$s, with a highly nonuniform profile at $t = 6$ $\mu$s. As the compression wave reaches the rear of the water column, it reflects as an expansion wave, with little trace of transmitting into the air; the wave essentially propagates back and forth inside the water, yielding a very-low-pressure region in the rear portion of the water, at $t = 10$ and 15 $\mu$s. It is interesting to note that the airflow outside the water column by and large develops independently from the water region, receiving little feedback; it mostly reacts to the shape of water column, which will change eventually as the wave structure inside the water is deforming its shape. The flow inside also evolves as though it were present in a container, but it is continuingly being influenced/modulated by the shock wave transmitted at the water/air interface as the foot of the incident shock wave is glancing over the interface.

## VI. Conclusions

In this paper, we have addressed a broad range of numerical issues inherent to the effective multifluid models: specifically, those pertinent to nonconservative terms, hyperbolicity, and stiffness. We focused on the hyperbolicity condition by the interfacial-pressure model. To achieve an accurate and robust solution of the complex system with disparate velocity and material scales, we developed a simple physics-inspired method that is applicable to fluids with general equations of state, having a distinct feature of not resorting to the details of the eigensystem. Numerical studies indicate that hyperbolicity is overarching in all nonlinear problems considered. As long as the compatibility for capturing stationary contact is handled properly, the nonconservative form does not seem to cause issues in stability, convergence, or the ability to capture sharp discontinuities.

## Appendix A: Characteristics Analysis

To study hyperbolicity of the two-fluid equations given in Eq. (1), it is simpler to arrive at the eigenvalue equation by employing the primitive variables:

$$\mathbf{Q} = (\alpha_1, p, u_1, u_2, \rho_1, \rho_2)^T \tag{A1}$$

The balance equation (1) is now written as

$$\mathbf{A}\frac{\partial \mathbf{Q}}{\partial t} + \mathbf{B}\frac{\partial \mathbf{Q}}{\partial x} = \mathbf{C}_t\frac{\partial \mathbf{Q}}{\partial t} + \mathbf{C}_x\frac{\partial \mathbf{Q}}{\partial x} \tag{A2}$$

where $\mathbf{A}$ and $\mathbf{B}$ are the usual Jacobians and $\mathbf{C}_t$ and $\mathbf{C}_x$ are the components associated with time and space derivatives of $\mathbf{P}^{\text{int}}$ and/or $\mathbf{F}^{\text{vm}}$, respectively. For completeness, they are given next:

$$\mathbf{A} = \begin{bmatrix} \rho_1 & 0 & 0 & 0 & \alpha_1 & 0 \\ -\rho_2 & 0 & 0 & 0 & 0 & \alpha_2 \\ \rho_1 u_1 & 0 & \alpha_1\rho_1 & 0 & \alpha_1 u_1 & 0 \\ -\rho_2 u_2 & 0 & 0 & \alpha_2\rho_2 & 0 & \alpha_2 u_2 \\ \rho_1 E_1 & \eta_1\alpha_1\rho_1 & \alpha_1\rho_1 u_1 & 0 & \alpha_1\Theta_1 & 0 \\ -\rho_2 E_2 & \eta_2\alpha_2\rho_2 & 0 & \alpha_2\rho_2 u_2 & 0 & \alpha_2\Theta_2 \end{bmatrix} \tag{A3}$$

$$\mathbf{B} = \begin{bmatrix} \rho_1 u_1 & 0 & \alpha_1\rho_1 & 0 & \alpha_1 u_1 & 0 \\ -\rho_2 u_2 & 0 & 0 & \alpha_2\rho_2 & 0 & \alpha_2 u_2 \\ \zeta_1 & \alpha_1 & 2\alpha_1\rho_1 u_1 & 0 & \alpha_1 u_1^2 & 0 \\ -\zeta_2 & \alpha_2 & 0 & 2\alpha_2\rho_2 u_2 & 0 & \alpha_2 u_2^2 \\ u_1\rho_1 H_1 & \alpha_1 u_1(1+\eta_1\rho_1) & \alpha_1(\zeta_1+\rho_1 E_1) & 0 & \alpha_1 u_1\Theta_1 & 0 \\ -u_2\rho_2 H_2 & \alpha_2 u_2(1+\eta_2\rho_2) & 0 & \alpha_2(\zeta_2+\rho_2 E_2) & 0 & \alpha_2 u_2\Theta_2 \end{bmatrix} \tag{A4}$$

$$\mathbf{C}_t = \begin{bmatrix} 0 & 0 & 0 & 0 & 0 & 0 \\ 0 & 0 & 0 & 0 & 0 & 0 \\ 0 & 0 & 0 & 0 & 0 & 0 \\ 0 & 0 & 0 & 0 & 0 & 0 \\ -p^{\text{int}} & 0 & 0 & 0 & 0 & 0 \\ p^{\text{int}} & 0 & 0 & 0 & 0 & 0 \end{bmatrix} \quad \mathbf{C}_x = \begin{bmatrix} 0 & 0 & 0 & 0 & 0 & 0 \\ 0 & 0 & 0 & 0 & 0 & 0 \\ p^{\text{int}} & 0 & 0 & 0 & 0 & 0 \\ -p^{\text{int}} & 0 & 0 & 0 & 0 & 0 \\ (p^{\text{int}}-p)u_1 & 0 & 0 & 0 & 0 & 0 \\ -(p^{\text{int}}-p)u_2 & 0 & 0 & 0 & 0 & 0 \end{bmatrix} \tag{A5}$$

where $E_k = e_k + u_k^2/2$, $H_k = E_k + p/\rho_k$, $\eta_k = \partial e_k/\partial p|_{\rho_k}$, $\chi_k = \partial e_k/\partial \rho_k|_p$, $\zeta_k = p + \rho_k u_k^2$, and $\Theta_k = E_k + \chi_k\rho_k$ $(k = 1, 2)$.

Equation (A2) is now grouped as

$$(\mathbf{A}-\mathbf{C_t})\frac{\partial \mathbf{Q}}{\partial \mathbf{t}} + (\mathbf{B}-\mathbf{C_x})\frac{\partial \mathbf{Q}}{\partial \mathbf{x}} = \mathbf{0} \tag{A6}$$

For the preceding system of PDEs to be hyperbolic, it is necessary that all roots of the characteristic polynomial resulting from the following matrix are real-valued:

$$|\mathbf{D} - \lambda\mathbf{I}| = \mathbf{0} \tag{A7}$$

where $\mathbf{D} = (\mathbf{A}-\mathbf{C}_t)^{-1}(\mathbf{B}-\mathbf{C}_x)$. It is interesting to note that the matrix $\mathbf{D}$ has two simple eigenvalues; they are associated with the velocities of both fluids $(u_1, u_2)$. That is, $\mathbf{D}$ has a structure given as

$$\mathbf{D} = \begin{bmatrix} \mathbf{G} & 0 & 0 \\ \cdots & u_1 & 0 \\ \cdots & 0 & u_2 \end{bmatrix} \tag{A8}$$

where the submatrix $\mathbf{G}$ is

$$\mathbf{G} = \begin{bmatrix} u_2 + \alpha_2\rho_1\Delta u\Gamma/a_2^2 & \alpha_1\alpha_2\Delta u\Gamma/(a_1a_2)^2 & \alpha_1\alpha_2\rho_1\Gamma/a_2^2 & -\alpha_1\alpha_2\rho_2\Gamma/a_1^2 \\ \rho_1\rho_2\Delta u\Gamma & u_1 - \alpha_2\rho_1\Delta u\Gamma/a_2^2 & \alpha_1\rho_1\rho_2\Gamma & \alpha_2\rho_1\rho_2\Gamma \\ \delta p/\alpha_1\rho_1 & 1/\rho_1 & u_1 & 0 \\ -\delta p/\alpha_2\rho_2 & 1/\rho_2 & 0 & u_2 \end{bmatrix} \tag{A9}$$

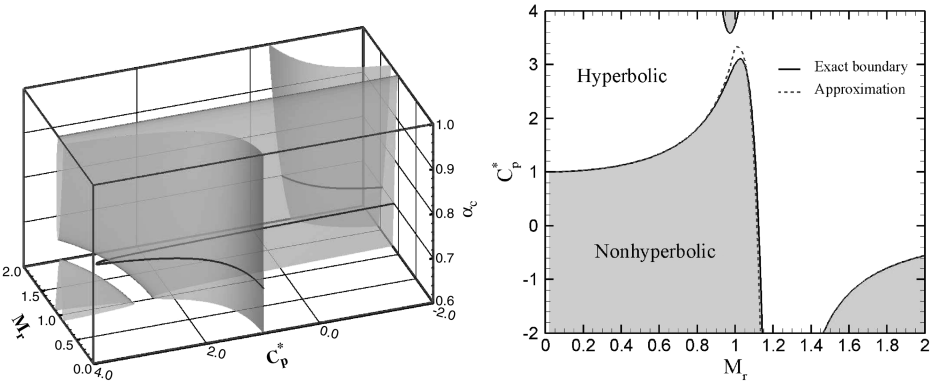


**Fig. A1 Hyperbolicity map of exact and approximate boundaries: $C_p^*(\alpha_c, M_r)$ (left) and $C_p^*(\alpha_c, M_r)$ (right) on a plane of $\alpha_c = 0.7$, where subscript $c$ denotes the continuous phase.**

where

$$\Gamma = \frac{a_1^2 a_2^2}{\alpha_1 \rho_2 a_2^2 + \alpha_2 \rho_1 a_1^2}, \qquad \Delta u = u_1 - u_2$$
$$a_k^2 = \left.\frac{\partial p}{\partial \rho_k}\right|_s, \qquad k = 1, 2 \tag{A10}$$

Hence, $|\mathbf{G} - \lambda \mathbf{I}| = \mathbf{0}$ produces a quartic characteristic polynomial, for which the zeros can be found by a standard procedure [25].

The hyperbolicity region expressed in the form of $C_p^*(\alpha_c, M)$ for a typical multiphase flow in various conditions is illustrated in Fig. A1, in which the values of $C_p^*$ demarcating hyperbolic and nonhyperbolic regions are depicted. It is noted that as the relative Mach number between two phases is increased, the amount of $C_p^*$ needed for maintaining hyperbolicity increases especially rapidly in the transonic region, acquiring a maximum value slightly past the sonic point.

An approximate analytical form of the boundary for a dilute liquid dispersal flow ($\alpha_g = 0.7$) is derived in another paper [11]. The curve of the approximate solution is also shown in Fig. A1, confirming a rather close approximation.

It must be cautioned that the preceding hyperbolicity consideration, as carried out, is purely a mathematical one, but the term (interfacial pressure in our case) that plays the central role is indeed based on physical consideration. However, no information about how big or how small the coefficient $C_p^*$ should be is available, which must come from experimental measurements. As seen in Fig. A1, hyperbolicity in the transonic range requires a value of $C_p^*$ that results in a physically unrealistic $p^{\text{int}} < 0$, because $\delta p^*$ exceeds the bulk static pressure. Hence, further development in this regard is still needed. Although the saga of modeling the interfacial-pressure term is yet to be closed, the preceding analysis is, by all means, useful in the context of a numerical solution with respect to stability and convergence.

## References


[1] Ishii, M., *Thermo-Fluid Dynamic Theory of Two-Phase Flow*, Eyrolles, Paris, 1975.

[2] Drew, D., and Passman, S., *Theory of Multicomponent Fluids*, Springer–Verlag, New York, 1999.

[3] Chang, C.-H., and Liou, M.-S., "A New Approach to the Simulation of Compressible Multifluid Flows with AUSM+ Scheme," AIAA Paper 03–4107, 2003.

[4] Chang, C.-H., and Liou, M.-S., "Simulation of Multifluid Multiphase Flows with AUSM$^+$-Up Scheme," *Computational Fluid Dynamics 2004*, Springer, Berlin, July 2004, pp. 613–618.

[5] Chang, C.-H., and Liou, M.-S., "A Robust and Accurate Approach to Computing Compressible Multiphase Flow: Stratified Flow Model and AUSM$^+$-Up Scheme," *Journal of Computational Physics*, Vol. 225, No. 1, 2007, pp. 840–873. doi:10.1016/j.jcp.2007.01.007

[6] Maso, G. D., LeFloch, P. G., and Murat, F., "Definition and Weak Stability of Nonconservative Products," *Journal de Mathématiques Pures et Appliquées*, Vol. 74, No. 6, 1995, pp. 483–548.

[7] Alouges, F., and Merlet, B., "Approximate Shock Curves of Nonconservative Hyperbolic Equations in One Space Dimension," *Journal of Hyperbolic Differential Equations*, Vol. 1, No. 4, 2004, pp. 769–788. doi:10.1142/S0219891604000251

[8] Stewart, H. B., and Wendroff, B., "Two-Phase Flow: Models and Methods," *Journal of Computational Physics*, Vol. 56, No. 3, 1984, pp. 363–409. doi:10.1016/0021-9991(84)90103-7

[9] Stuhmiller, J., "The Influence of Interfacial Pressure Forces on the Character of Two-Phase Flow Model Equations," *International Journal of Multiphase Flow*, Vol. 3, No. 6, 1977, pp. 551–560. doi:10.1016/0301-9322(77)90029-5

[10] Liou, M.-S., Nguyen, L., Chang, C.-H., Sushchikh, S., Nourgaliev, R., and Theofanous, T., "Hyperbolicity, Discontinuities, and Numerics of Two-Fluid Models," *4th International Conference on Computational Fluid Dynamics*, Gent, Belgium, July 2006.

[11] Chang, C.-H., Sushchikh, S., Nguyen, L., Liou, M.-S., and Theofanous, T., "Hyperbolicity, Discontinuities, and Numerics of the Two-Fluid Model," 5th Joint ASME/JSME Fluids Engineering Summer Conference, American Society of Mechanical Engineers, Fluid Engineering Div., Paper FEDSM2007-37338, 2007.

[12] Harlow, F., and Amsden, A., "Fluid Dynamics," Los Alamos Scientific Lab., Rept. LA-4700, Los Alamos, NM, 1971.

[13] Abgrall, R., "How to Prevent Pressure Oscillations in Multicomponent Flow Calculations: A Quasi Conservative Approach," *Journal of Computational Physics*, Vol. 125, No. 1, 1996, pp. 150–160. doi:10.1006/jcph.1996.0085

[14] Keyfitz, B., Sanders, R., and Sever, M., "Lack of Hyperbolicity in the Two-Fluid Model for Two-Phase Incompressible Flow," *Discrete and Continuous Dynamical Systems. Series B.*, Vol. 3, No. 4, 2003, pp. 541–563.

[15] Keyfitz, B., Sever, M., and Zhang, F., "Viscous Singular Shock Structure for a Nonhyperbolic Two-Fluid Model," *Nonlinearity*, Vol. 17, No. 5, 2004, pp. 1731–1747. doi:10.1088/0951-7715/17/5/010

[16] Toumi, I., "An Upwind Numerical Method for Two-Flow Two-Phase Flow Models," *Nuclear Science and Engineering*, Vol. 123, No. 2, 1996, pp. 147–168.

[17] Städtke, H., Franchello, G., and Worth, B., "Numerical Simulation of Multi-Dimensional Two-Phase Flows Based on Flux Vector Splitting," *Nuclear Engineering and Design*, Vol. 177, Nos. 1–3, 1997, pp. 199–213. doi:10.1016/S0029-5493(97)00194-5

[18] Saurel, R., and Abgrall, R., "A Multiphase Godunov Method for Compressible Multifluid and Multiphase Flows," *Journal of Computational Physics*, Vol. 150, No. 2, 1999, pp. 425–467. doi:10.1006/jcph.1999.6187

[19] Liou, M.-S., and Steffen, C. J., "A New Numerical Flux," *Journal of Computational Physics*, Vol. 107, No. 1, 1993, pp. 23–39. doi:10.1006/jcph.1993.1122

[20] Liou, M.-S., "A Sequel to AUSM: AUSM$^+$," *Journal of Computational Physics*, Vol. 129, No. 2, 1996, pp. 364–382. doi:10.1006/jcph.1996.0256

[21] Liou, M.-S., "A Sequel to AUSM, Part 2: AUSM$^+$-Up for All Speeds,," *Journal of Computational Physics*, Vol. 214, No. 1, 2006, pp. 137–170. doi:10.1016/j.jcp.2005.09.020

[22] Niu, Y.-Y., "Advection Upwinding Splitting Method to Solve a Compressible Two-Fluid Model," *International Journal for Numerical Methods in Fluids*, Vol. 36, No. 3, 2001, pp. 351–371. doi:10.1002/fld.138

[23] Paillère, H., Corre, C., and Cascales, J. R. G., "On the Extension of the AUSM$^+$ Scheme to Compressible Two-Fluid Models," *Computers and Fluids*, Vol. 32, No. 6, 2003, pp. 891–916. doi:10.1016/S0045-7930(02)00021-X

[24] Theofanous, T. G., Nguyen, L., and Chang, C.-H., "Documentation of ARMS Code," Center for Risk Studies and Safety, Univ. of California, Santa Barbara, Santa Barbara, CA, 2008.

[25] Abramovitz, M., and Stegun, I. A. (eds.), "Solutions of Quartic Equations," *Handbook of Mathematical Functions with Formulas, Graphs, and Mathematical Tables*, Dover, New York, 1972, pp. 17–18.


K. Powell
*Associate Editor*